

# Performance optimization of lead-free KGeCl<sub>3</sub> based perovskite solar cells using SCAPS-1D

Rahul Kundara \* , Sarita Baghel

*Department of Applied Physics, Delhi Technological University, Delhi, India*

## ARTICLE INFO

Handling editor: 'Ranga Pitchumani'

**Keywords:**  
KGeCl<sub>3</sub>-based PSC  
SCAPS-1D  
ETLs and HTLs

## ABSTRACT

The commercial application of lead-based Perovskite Solar Cells (PSCs) is restrained by their toxicity. In this work, we have investigated KGeCl<sub>3</sub> which is a potential candidate for non-lead PSC. SCAPS-1D software is employed to examine the impact of distinct Hole Transport Layers (HTLs), absorber layer and Electron Transport Layers (ETLs) to maximize the device performance. The effect of absorber layer thickness, its acceptor and donor concentration (N<sub>A</sub> and N<sub>D</sub>) have been analyzed. We have obtained a maximum efficiency of 29.82 % with open circuit voltage (V<sub>OC</sub>) = 1.19 V, short circuit current density (J<sub>SC</sub>) = 30.08 mA/cm<sup>2</sup>, and fill factor (FF) = 82.74 % for the configuration of FTO/WS<sub>2</sub>/KGeCl<sub>3</sub>/PEDOT: PSS/Au at radiative recombination coefficient of 10<sup>-12</sup> cm<sup>3</sup>/sec, operating temperature of 300 K and defect density of 10<sup>15</sup> cm<sup>-3</sup>. The optimized thickness of the absorber layer is 600 nm. Thus, the investigation suggests that WS<sub>2</sub> as ETL and PEDOT: PSS as HTL is most suitable for the Ge-based PSC. Hence, this configuration is most suitable to manufacture highly efficient PSC devices.

## 1. Introduction

Global warming, rapid industrialization and growing population will drive the demand for renewable sources of energy which should also be environment friendly. In this scenario solar energy devices offer a clean and sustainable solution for the increase in energy demand. Currently Silicon based Photovoltaic (PV) modules dominate the solar cell market due to their stable and efficient performance. But the Silicon technology is not completely environment friendly when analyzed through its complete life cycle assessment. They are difficult to recycle and they have high carbon emission during the production stage. However, perovskite solar cells (PSCs) are the emerging class of photovoltaics due to its promising properties such as tunable bandgap (E<sub>g</sub>), high absorption coefficient, low manufacturing cost and low temperature fabrication. Perovskite material has an ABX<sub>3</sub> structure (where A is an organic or inorganic cation, B is an inorganic metal cation and X is halogen anion) [1]. In the typical structure of a PSC, the absorber layer is positioned between Electron Transport Layer (ETL) and Hole Transport Layer (HTL). The generation of photocurrent occurs through injection of photoelectrons into the ETL and the transfer holes through the HTL from the absorber layer. Therefore, ensuring appropriate alignment of the energy band levels across the layers is essential for achieving optimal device performance.

In 2009, PSC was reported with an efficiency of 3.8 % and has achieved maximum power conversion efficiency (PCE) approximately 26 % till now for CH(NH<sub>2</sub>)<sub>2</sub>PbI<sub>3</sub> and CH<sub>3</sub>NH<sub>3</sub>PbI<sub>3</sub> perovskite materials [2,3,4,5]. Recently various hybrid organic-inorganic perovskite materials have been reported which possess high charge carrier mobilities and also offer low temperature solution-based fabrication techniques [6,7,8]. They possess some challenges related to stability, toxicity and scalability [9]. The inorganic PSCs, particularly those employing materials like cesium lead halides have advantages over hybrid PSCs as follows: improved stability, scalability and non-toxic alternatives [10,11] but they have phase stability issues and complexity in fabrication [12]. It is mostly lead (Pb)-based PSCs [3,4,5] that have demonstrated experimental PCE of 20.17 % for CsPbI<sub>3</sub> [13]. But, despite the high performance of Pb based PSC, its stability is a major challenge. There are many degradation reactions which impact the PV performance and device stability. There is instability due to rapid oxidation of Pb cation, interfacial reactions of Pb with other materials in the device [14]. Apart from this toxicity concerns also need to be addressed. Though Pb is a toxic substance, there are recent studies which indicate that its use in PSC is limited to less than 1 gm/m<sup>2</sup> which can be easily managed by proper encapsulation and appropriate recycling systems [15]. On the other hand, the effect of toxicity of lead versus non-lead PSCs have also been investigated [16] and the studies show that, due

\* Corresponding author.

E-mail address: [rahul\\_2k20phdap10@dtu.ac.in](mailto:rahul_2k20phdap10@dtu.ac.in) (R. Kundara).

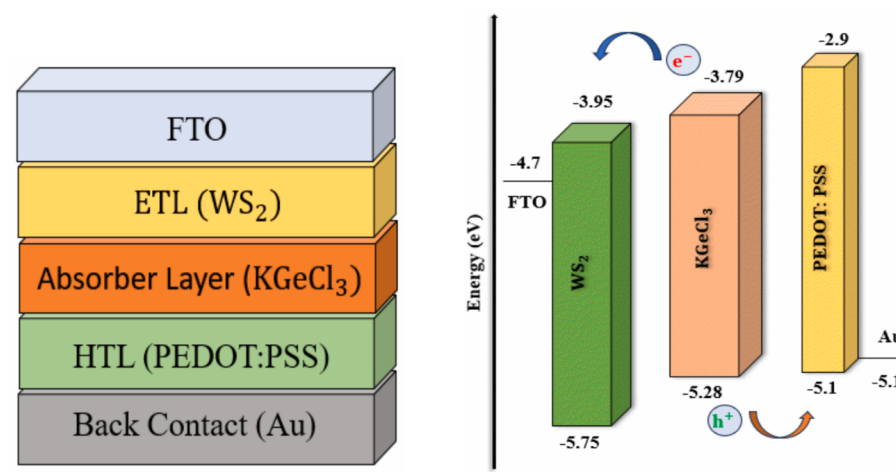


**Fig. 1.** Architecture and band alignment diagram for KGeCl<sub>3</sub> PSC.

**Table 1**  
Input parameters were used in simulation of distinct ETLs.

Parameter	CdS [27]	PCBM [28,29]	C <sub>60</sub> [30]	WS <sub>2</sub> [31]	KGeCl <sub>3</sub> [32]
Thickness (μm)	0.050	0.500	0.050	0.100*	0.300
E <sub>g</sub> (eV)	2.42	2.1	1.7	1.8	1.49
χ (eV)	4.3	3.9	3.9	3.95	3.52
ε <sub>r</sub>	9.35	3.9	4.2	13.6	3.52
N <sub>C</sub> (cm <sup>-3</sup> )	2.2 × 10 <sup>18</sup>	2.2 × 10 <sup>19</sup>	8.0 × 10 <sup>18</sup>	1 × 10 <sup>18</sup>	1 × 10 <sup>18</sup>
N <sub>V</sub> (cm <sup>-3</sup> )	1.8 × 10 <sup>19</sup>	2.2 × 10 <sup>19</sup>	8.0 × 10 <sup>19</sup>	2.4 × 10 <sup>19</sup>	1 × 10 <sup>19</sup>
μ <sub>n</sub> (cm <sup>2</sup> /Vs)	100	0.001	8.0 × 10 <sup>-2</sup>	100	20
μ <sub>p</sub> (cm <sup>2</sup> /Vs)	25	0.002	3.5 × 10 <sup>-3</sup>	100	20
N <sub>D</sub> (cm <sup>-3</sup> )	1.15 × 10 <sup>17</sup>	1 × 10 <sup>19</sup>	2.6 × 10 <sup>17</sup>	1 × 10 <sup>18</sup>	1 × 10 <sup>15</sup>
N <sub>A</sub> (cm <sup>-3</sup> )	0	—	—	0	1 × 10 <sup>15</sup>
N <sub>t</sub> (cm <sup>-3</sup> )	1 × 10 <sup>15*</sup>	1 × 10 <sup>9*</sup>	1 × 10 <sup>14</sup>	1 × 10 <sup>13*</sup>	1 × 10 <sup>13</sup>

\*In this work.

to the toxic nature of lead, there is a need to find environmentally friendly substitutes for it. However, before doing so, one has to consider the results of life cycle assessment studies of available alternative materials. There have been various investigations to substitute hazardous Pb ions with other alternatives such as Sn [17], Ge [18], Bi [19], Sb [20] and Ag [21]. But most of the alternatives do not offer substantial advantages in terms of cost, toxicity or environmental safety. Recently reported DFT study shows that KGeCl<sub>3</sub> is a promising perovskite material for PV application [Namisi et al. 2023]. There are very few experimental or theoretical investigations on KGeCl<sub>3</sub> for solar cell application

so far. The study comprises the application of KGeCl<sub>3</sub> as a perovskite material and simulated the PSC using SCAPS-1D. The recently reported studies demonstrated that KGeCl<sub>3</sub>-based PSC achieved a PCE of 15.83 % [22] and 19.62 % [23] using SCAPS-1D. Previously germanium-based double PSC has been simulated and obtained a maximum PCE of 22.5 % [24] whereas MAGeI<sub>3</sub>-based PSC has achieved a theoretical PCE of 25.34 % [25]. SnGe-based PSC has been theoretically obtained at an efficiency of 24.20 % [26]. We have simulated the various ETLs (CdS, PCBM, C<sub>60</sub> and WS<sub>2</sub>) and HTLs (CuI, Spiro-OMeTAD, Cu<sub>2</sub>O, PEDOT: PSS and MoS<sub>2</sub>) and analyzed the effects on the PV parameters of PSC. The optimization of thickness of absorber layer, operating temperature, energy band gap (E<sub>g</sub>) and carrier concentration (N<sub>D</sub>, N<sub>A</sub>) have been done to achieve the maximum PCE. The simulated KGeCl<sub>3</sub> device achieved a highest PCE of 29.82 % (with V<sub>OC</sub> = 1.19 V, J<sub>SC</sub> = 30.08 mA/cm<sup>2</sup>, and FF = 82.74 %) at 300 K with WS<sub>2</sub> as ETL and PEDOT: PSS as HTL. These photovoltaic outcomes showed that KGeCl<sub>3</sub> is promising material to fabricate lead-free low cost and efficient PSCs.

## 2. Material and Methods

### 2.1. Device architecture

The Fig. 1 depicts the device architecture and band alignment of the KGeCl<sub>3</sub>-based PSC. The PSC structure typically includes distinct layers, an absorber layer situated between ETL and HTL. The gold (Au) is chosen as a back contact electrode with a work function of 5.1 eV. During the simulation of the Ge-based PSC, different ETLs and HTLs are simulated to determine the optimal combination that yields the maximum PCE while also optimizing the thickness of the absorber layer. The thickness of various ETLs (CdS, PCBM, C<sub>60</sub> and WS<sub>2</sub>) varies from 50 nm to 500 nm shown below in Table 1. The employed KGeCl<sub>3</sub> absorber

**Table 2**  
Input parameters used in simulation of various HTLs.

Parameter	FTO [33,34]	CuI [35]	Spiro-OMeTAD [36,37]	Cu <sub>2</sub> O [33,35]	PEDOT: PSS [28,30]	MoS <sub>2</sub> [38]
Thickness (μm)	0.400	0.100	0.213	0.250 0.080	—	0.200
E <sub>g</sub> (eV)	3.5	3.1	3	2.17 2.2	—	1.29
χ (eV)	4.0	2.1	2.2	3.2 2.9	—	4.2
ε <sub>r</sub>	9.0	6.5	3	7.11 3.0	—	3.0
N <sub>C</sub> (cm <sup>-3</sup> )	2.02 × 10 <sup>18</sup>	2.8 × 10 <sup>19</sup>	1 × 10 <sup>19</sup>	2.02 × 10 <sup>17</sup> 2.2 × 10 <sup>15</sup>	—	2.2 × 10 <sup>18</sup>
N <sub>V</sub> (cm <sup>-3</sup> )	1.8 × 10 <sup>19</sup>	1 × 10 <sup>19</sup>	1 × 10 <sup>19</sup>	1.1 × 10 <sup>19</sup> 1.8 × 10 <sup>18</sup>	—	1.8 × 10 <sup>19</sup>
μ <sub>n</sub> (cm <sup>2</sup> /Vs)	20	100	10 <sup>-4</sup>	200 1 × 10 <sup>-2</sup>	—	100
μ <sub>p</sub> (cm <sup>2</sup> /Vs)	10	43.9	10 <sup>-4</sup>	80 2 × 10 <sup>-4</sup>	—	150
N <sub>D</sub> (cm <sup>-3</sup> )	2 × 10 <sup>19</sup>	—	—	—	—	1 × 10 <sup>15</sup>
N <sub>A</sub> (cm <sup>-3</sup> )	0	1 × 10 <sup>18</sup>	2 × 10 <sup>19</sup>	1 × 10 <sup>18</sup> 10 <sup>19</sup>	—	1 × 10 <sup>17</sup>
N <sub>t</sub> (cm <sup>-3</sup> )	1 × 10 <sup>15</sup>	1 × 10 <sup>14</sup>	1 × 10 <sup>14</sup>	1 × 10 <sup>14</sup> 1 × 10 <sup>14</sup>	—	1 × 10 <sup>14</sup>

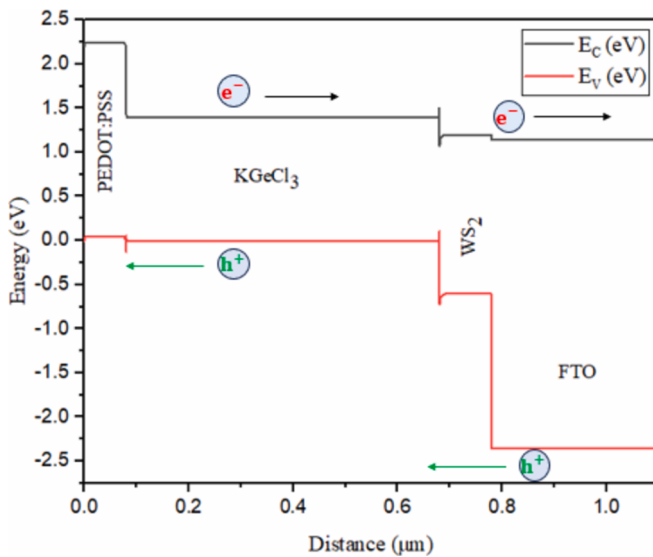


**Fig. 2.** Energy band diagram of FTO/WS<sub>2</sub>/KGeCl<sub>3</sub>/PEDOT: PSS/Au PSC.

**Table 3**

KGeCl<sub>3</sub> PSC performance before optimization (at thickness of absorber layer = 300 nm, E<sub>g</sub> = 1.49 eV, N<sub>D</sub> = N<sub>A</sub> = 1 × 10<sup>14</sup> cm<sup>-3</sup> and N<sub>t</sub> = 10<sup>13</sup> cm<sup>-3</sup>) with different ETLs and HTLs.

Device architecture	V <sub>OC</sub> (V)	J <sub>SC</sub> (mA/cm <sup>2</sup> )	FF (%)	PCE (%)
FTO/C <sub>60</sub> /KGeCl <sub>3</sub> /Spiro-OMeTAD/Au	1.30	22.60	80.39	23.63
FTO/C <sub>60</sub> /KGeCl <sub>3</sub> /PEDOT: PSS/Au	1.30	22.67	80.49	23.74
FTO/C <sub>60</sub> /KGeCl <sub>3</sub> /Cu <sub>2</sub> O/Au	1.30	22.80	80.56	23.90
FTO/WS <sub>2</sub> /KGeCl <sub>3</sub> /MoS <sub>2</sub> /Au	1.02	23.04	81.11	19.09
FTO/WS <sub>2</sub> /KGeCl <sub>3</sub> /CuI/Au	1.31	23.10	84.41	25.57
FTO/WS <sub>2</sub> /KGeCl <sub>3</sub> /Spiro-OMeTAD/Au	1.31	23.10	84.22	25.51
FTO/WS <sub>2</sub> /KGeCl <sub>3</sub> /PEDOT: PSS/Au	1.31	23.15	84.36	<b>25.61</b>
FTO/WS <sub>2</sub> /KGeCl <sub>3</sub> /CuI/Au	1.31	23.10	84.41	25.57
FTO/CdS/KGeCl <sub>3</sub> /PEDOT: PSS/Au	1.30	22.50	74.98	22.05
FTO/WS <sub>2</sub> /KGeCl <sub>3</sub> /CBTS/Au	1.31	23.20	83.92	25.52
FTO/WS <sub>2</sub> /KGeCl <sub>3</sub> /CFTS/Au	1.12	25.34	87.86	25.01
FTO/PCBM/KGeCl <sub>3</sub> /Cu <sub>2</sub> O/Au	1.28	13.61	84.24	14.73

layer with thickness of 300 nm shown below in Table 1. Various HTLs are used to enhance the PCE of the PSC, including CuI, Spiro-OMeTAD, Cu<sub>2</sub>O, PEDOT: PSS and MoS<sub>2</sub> with thickness varying from 80 nm to 250 nm shown below in Table 2. The band alignment diagram of the optimized device shown below in Fig. 2 illustrates the transport of charge carriers, specifically the movement of photo-generated electrons (e<sup>-</sup>s) and holes (h<sup>+</sup>s) across the device. Electrons have propensity to migrate from higher to lower energy levels, transitioning from PEDOT: PSS (E<sub>C</sub> ~ 2.2 eV) to KGeCl<sub>3</sub> (with E<sub>C</sub> ranging from 0.05 to 1.50 eV), then WS<sub>2</sub> (E<sub>C</sub> ~ 1.2 eV), and ultimately to FTO (E<sub>C</sub> ~ 1.1 eV). Likewise, hole transport is facilitated by the configuration of valence levels. Holes have ability to migrate freely from FTO (E<sub>V</sub> ~ -2.36 eV) to WS<sub>2</sub> (E<sub>V</sub> ~ -0.60 eV), then to KGeCl<sub>3</sub> (E<sub>V</sub> ~ 0 eV), and finally to PEDOT: PSS (E<sub>V</sub> ~ 0.04 eV). At the interface of WS<sub>2</sub>/KGeCl<sub>3</sub>, a moderate upward cleavage is observed. Instead of being detrimental, this phenomenon acts as a barrier, preventing excessive photo-generated e<sup>-</sup>s and h<sup>+</sup>s from flowing through the conduction and valence bands, respectively. Such regulation is crucial as it helps prevent rapid current saturation. The simulated performance data of KGeCl<sub>3</sub> PSC before optimization with distinct ETLs and HTLs demonstrated in Table 3.

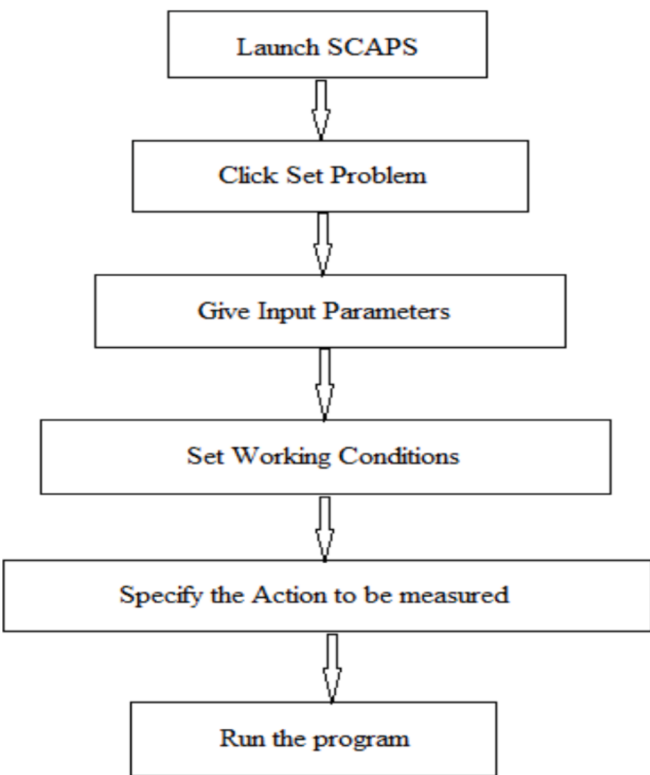


**Fig. 3.** Flow chart of simulation procedure.

## 2.2. Simulation Method

The data of different parameters are chosen from previous studies. The SCAPS-1D (version 3.3.10) has been employed for simulation. This software can be used for simulations at different input physical conditions. This tool calculation is dependent on differential equations, including Poisson's and continuity equations. It can calculate Quantum efficiency (QE), J-V curve and carrier lifetime for both e<sup>-</sup>s and h<sup>+</sup>s.

$$\frac{\partial^2 \psi}{\partial x^2} + \frac{q}{\epsilon} [p(x) - n(x) + N_D - N_A + \rho_p - \rho_n] = 0 \quad (1)$$

$$\frac{1}{q} \frac{dJ_p}{dx} = G_{op}(x) - R(x) \quad (2)$$

$$\frac{1}{q} \frac{dJ_n}{dx} = -G_{op}(x) + R(x) \quad (3)$$

The simulations were run at 300 K using a “air mass 1.5 global” spectrum and a light power of 1000 W/m<sup>2</sup>. The work is dependent on change in thickness, E<sub>g</sub>, N<sub>D</sub>, and N<sub>A</sub> at which simulation of the proposed PSC has been done. The outcome of the device has been reflected by the I-V characteristics which represent the following PV parameters: J<sub>SC</sub>, FF, V<sub>OC</sub>, and PCE. The simulation procedure is depicted in Fig. 3.

## 3. Results and discussion

### 3.1. Impact of distinct parameters on KGeCl<sub>3</sub>-based PSC

#### 3.1.1. Effect of bandgap with thickness

This section includes effect of the absorber layer thickness, E<sub>g</sub>, donor and acceptor carrier concentration (N<sub>D</sub> and N<sub>A</sub>) on PV parameters (V<sub>OC</sub>, J<sub>SC</sub>, FF and PCE) of KGeCl<sub>3</sub>-based PSC where thickness of absorber layer, bandgap, N<sub>D</sub> and N<sub>A</sub> are fixed at 0.3 μm, 1.49 eV and 10<sup>15</sup> cm<sup>-3</sup> respectively. The contour plot shown below in Fig. 4 demonstrates that change in PV parameters of simulated PSC as a function of thickness of

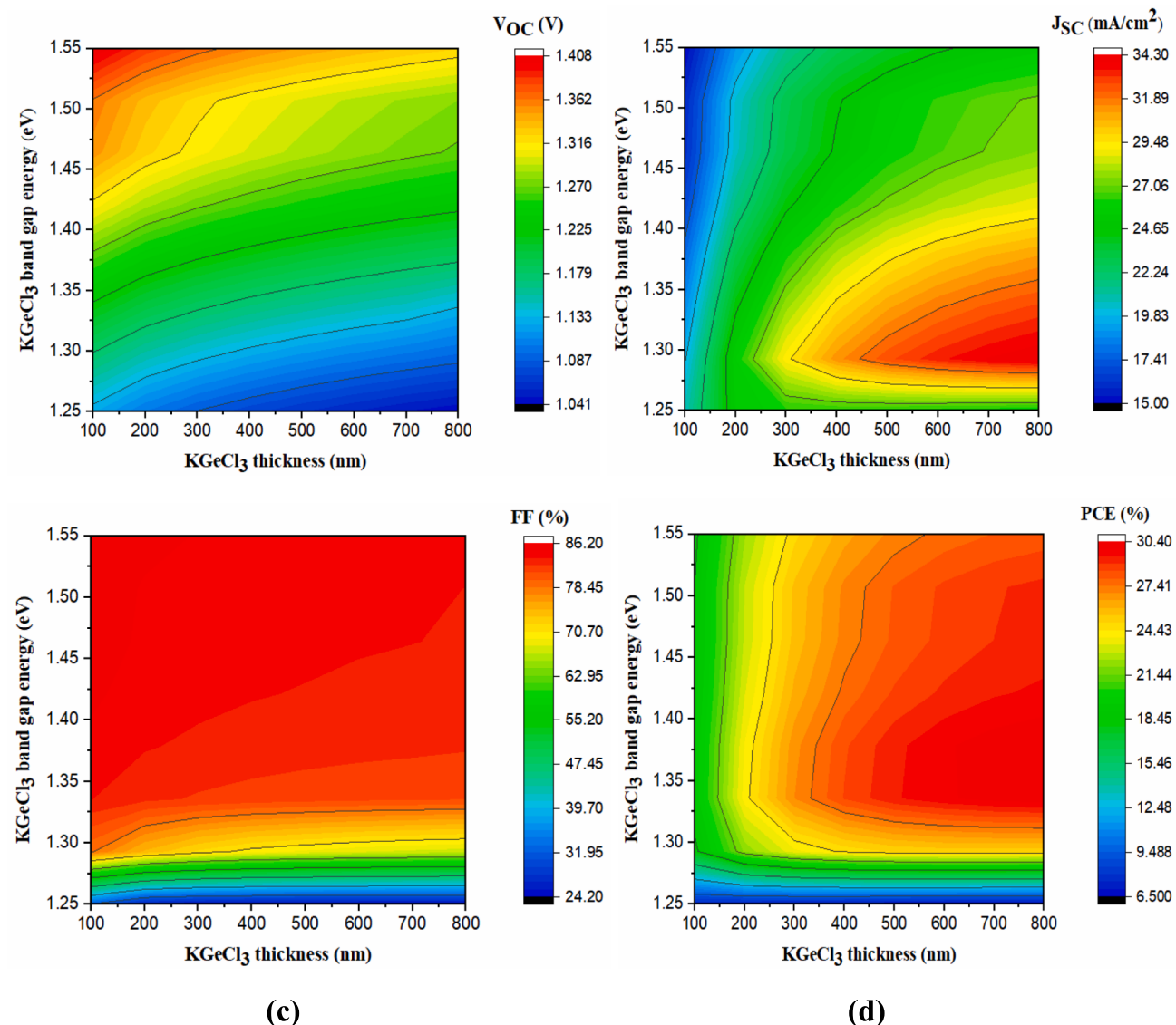


**Fig. 4.** Change in PV parameters of simulated PSC such as (a)  $V_{\text{OC}}$  (b)  $J_{\text{SC}}$  (c) FF and (d) PCE with thickness of absorber layer and bandgap at doping concentration of  $10^{15} \text{ cm}^{-3}$ .

$\text{KGeCl}_3$  and its  $E_g$  change from 100 to 800 nm and from 1.25 to 1.55 eV respectively. Fig. 4(a) shows that  $V_{\text{OC}}$  increases from 1.041 V at  $E_g$  of 1.25 eV to about 1.408 V at  $E_g$  of 1.55 eV while the change in  $V_{\text{OC}}$  with thickness rises from 100 to 800 nm. For Fig. 4 (a), a higher  $E_g$  leads to a higher  $V_{\text{OC}}$ , it allows a larger separation between the quasi-fermi levels of electrons and holes. It reduces thermal carrier generation and intrinsic recombination rates. The decrease in  $V_{\text{OC}}$  with increasing temperature can be attributed to the creation of more interfacial defects, an increase in series resistance, and a reduction in carrier diffusion length [39,40]. The value of  $J_{\text{SC}}$  falls from 34.30 to 15.09 mA/cm<sup>2</sup> with an increment in value of 1.25 to 1.55 eV depicted in Fig. 4(b). For Fig. 4 (b),  $J_{\text{SC}}$  has low values as  $E_g$  increases for the thickness between 100 to 300 nm. This is perhaps due to low charge carrier generation due to very small value of thickness. High value of  $J_{\text{SC}}$  obtained for thickness between 600 to 700 nm and at  $E_g$  of 1.30 eV. For the as  $E_g$  greater than 1.30 eV causes decreasing the absorption within the layer and hence  $J_{\text{SC}}$  decreases [41]. The value of  $J_{\text{SC}}$  increases for each thickness of  $\text{KGeCl}_3$ , ranging from 100 to 800 nm.

The Fig. 4(c) indicate that the FF was increased from 31.69 to 86.02 % with increment in the value of  $E_g$  from 1.25 to 1.55 eV and this with simultaneous increment in  $\text{KGeCl}_3$  thickness from 100-800 nm with

approximate decrement of 2.59 % in value of FF. The Fig. 4(d) depicted that the value of PCE was 6.89 % at  $E_g$  of 1.25 eV with increment in thickness of  $\text{KGeCl}_3$  from 100-800 nm at various regions. An average PCE of approximately 23.30 % is attained across variations of  $E_g$  ranging from 1.25 to 1.55 eV. Additionally, within a thickness range of 500 to 800 nm, a higher performance level of about 28.85 % is achieved. These findings can be elucidated as follows: with an increase in the  $E_g$ , there is a concurrent rise in the local collection of light absorption within the  $\text{KGeCl}_3$  thin film. These outcomes can be clarified by observing that as the  $E_g$  increases, the local collection efficiency of light absorption within the absorber layer increases. This enhancement augments the carrier generation rate, consequently leading to a dramatic increase in the  $V_{\text{OC}}$ , as indicated by the equation [42].

$$V_{\text{oc}} = \frac{k_B T}{q} \ln(1 + I_{\text{ph}} I_0) \quad (4)$$

Where  $V_{\text{OC}}$  is open circuit voltage,  $k_B$  is Boltzmann constant,  $T$  is temperature in K,  $q$  is electronic charge,  $I_{\text{ph}}$  is Photogenerated current and  $I_0$  is reverse saturation current. The outcomes suggest that to maximize the PCE in PSC, it is optimal to have a  $\text{KGeCl}_3$   $E_g$  of 1.40 eV and a thickness ranging from 500 to 800 nm. JV plots were simulated for PSCs varying

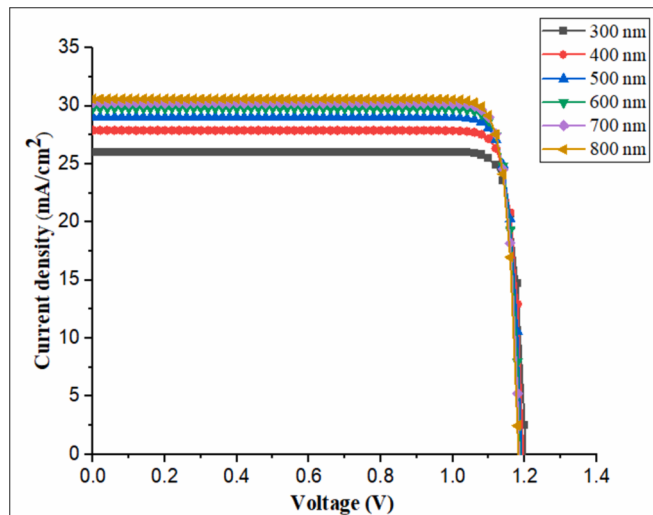


**Fig. 5.** The JV curves of the PSC with thickness of the absorber layer.

KGeCl<sub>3</sub> thickness ranging from 300 to 800 nm while maintaining a fixed E<sub>g</sub> of 1.40 eV, as depicted in Fig. 5. It is suggested that the E<sub>g</sub> should be tuned using suitable dopants to get this optimal value of band gap. These results reveal the following trends: V<sub>OC</sub> ranges between 1.18 V and 1.20 V, the J<sub>SC</sub> changes from 26.05 to 30.60  $\text{mA}/\text{cm}^2$ , FF remains constant at 89 % and PCE ranges from 28.06 to 29.82 % with increase in thickness of KGeCl<sub>3</sub> thickness. Notably, the PCE trend closely follows the variations in V<sub>OC</sub> and FF values.

### 3.1.2. Effect of donor carrier concentration ( $N_D$ ) with thickness

The Fig. 6 demonstrates the contour plot depicting the PV parameters as functions of the KGeCl<sub>3</sub> layer thickness varies 100 to 800 nm (x-axis) and N<sub>D</sub> ranging between  $1 \times 10^{14}$  to  $1 \times 10^{21}$   $\text{cm}^{-3}$  (y-axis) respectively. From Fig. 6(a), it is revealed that the V<sub>OC</sub> increases from approximately 0.96 to 1.41 V as the N<sub>D</sub> rises from  $1 \times 10^{14}$  to  $1 \times 10^{21}$   $\text{cm}^{-3}$ , with major fluctuations in the V<sub>OC</sub> values observed with increasing KGeCl<sub>3</sub> thickness. According to Fig. 6(b), the J<sub>SC</sub> value increases approximately 17.72 to 31.06  $\text{mA}/\text{cm}^2$  as N<sub>D</sub> rises from  $1 \times 10^{14}$  to  $1 \times 10^{19}$   $\text{cm}^{-3}$  and J<sub>SC</sub> remain constant at about 28.48  $\text{mA}/\text{cm}^2$  for KGeCl<sub>3</sub> thickness exceeding 400 nm. Conversely, for KGeCl<sub>3</sub> thickness below 400 nm, J<sub>SC</sub> maintains around 21.90  $\text{mA}/\text{cm}^2$  below N<sub>D</sub> of  $1 \times 10^{20}$   $\text{cm}^{-3}$ . Above N<sub>D</sub> of  $1 \times 10^{21}$   $\text{cm}^{-3}$ , the value of J<sub>SC</sub> falls to 0.37  $\text{mA}/\text{cm}^2$  irrespective of the KGeCl<sub>3</sub> thickness. Fig. 6(c) suggests that the FF

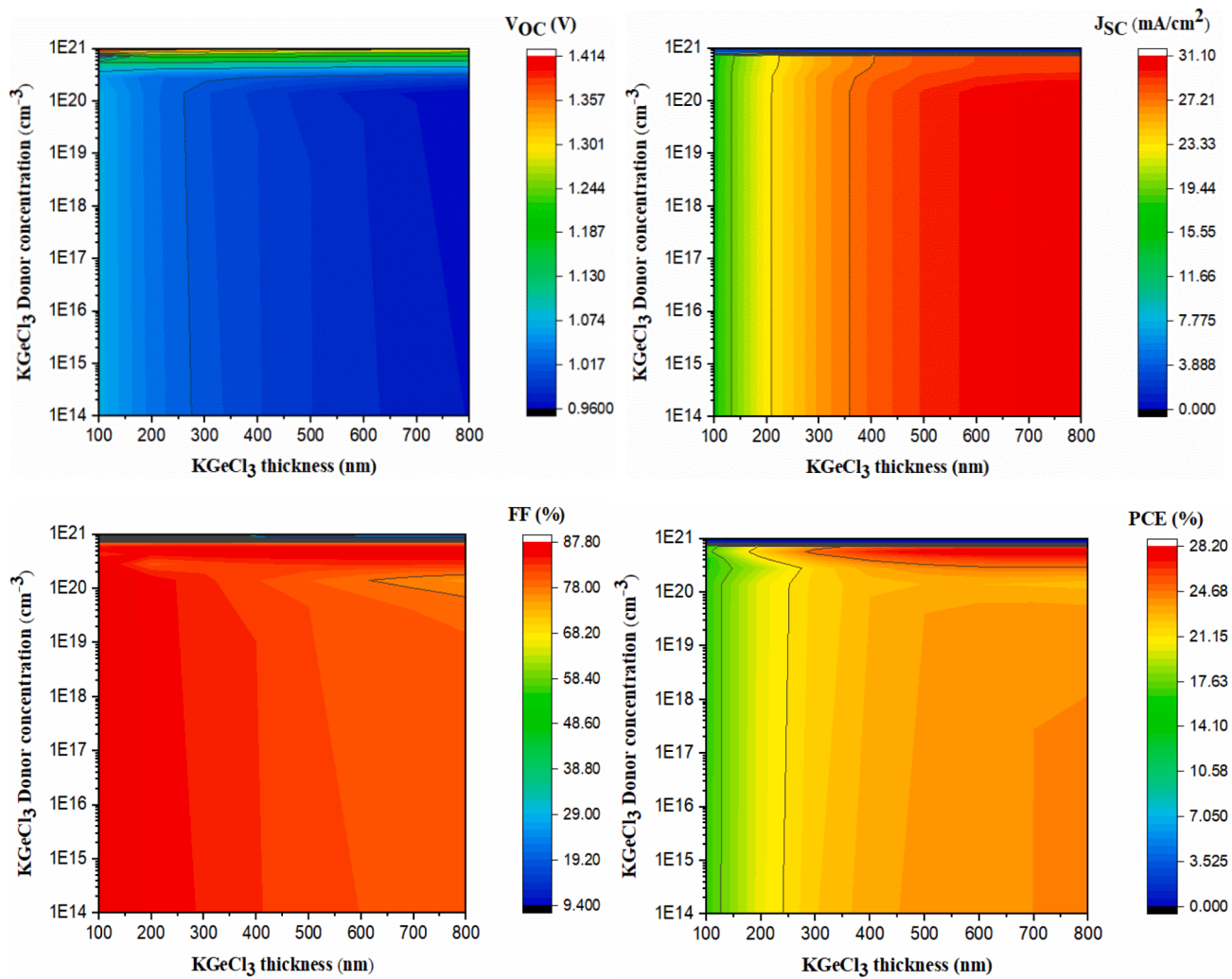


**Fig. 6.** Variation in PV parameters of simulated PSC such as (a) V<sub>OC</sub> (b) J<sub>SC</sub> (c) FF and (d) PCE with thickness of absorber layer and N<sub>D</sub> at E<sub>g</sub> = 1.40 eV.

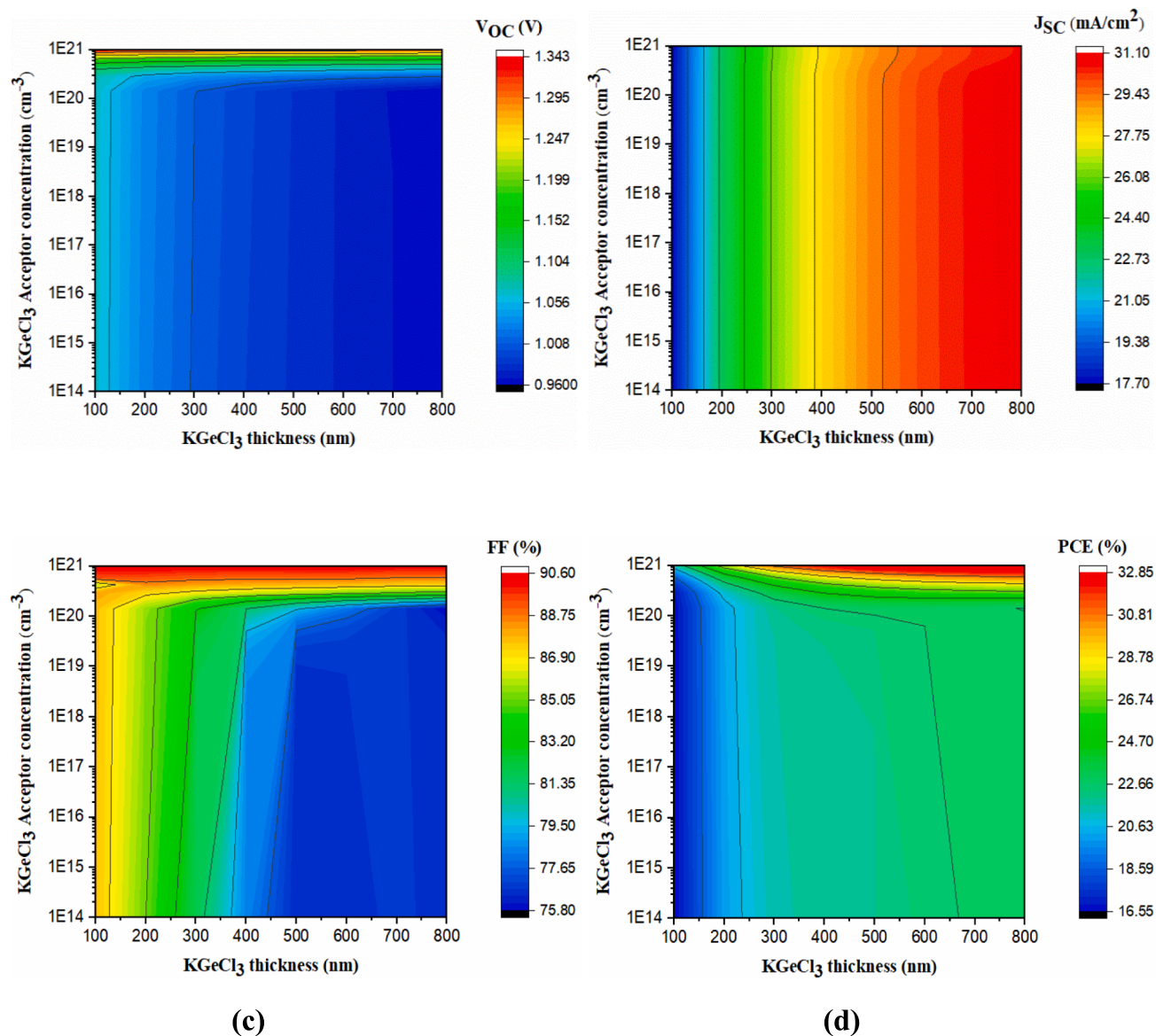


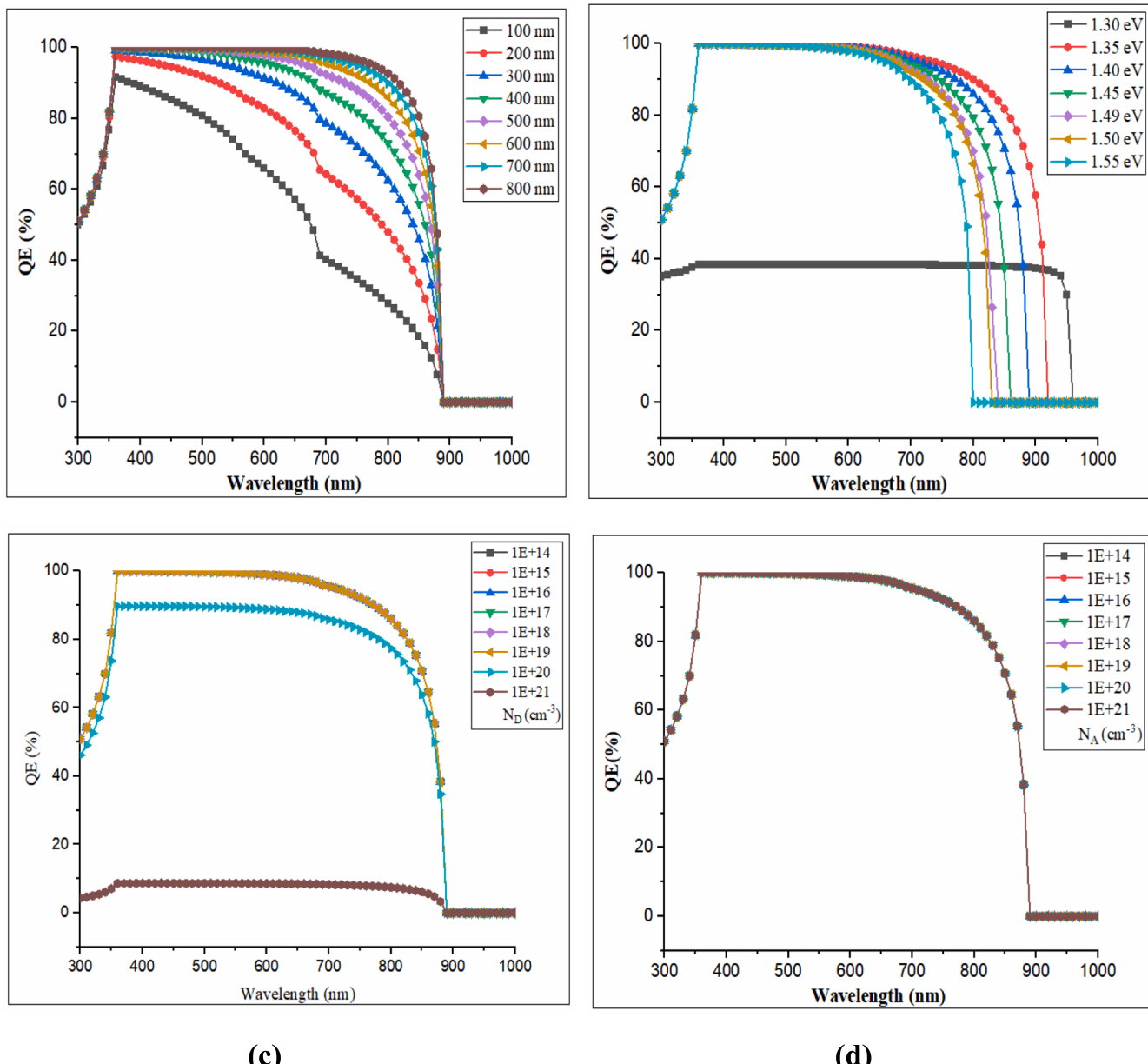
**Fig. 7.** Variation in PV parameters of simulated PSC such as (a)  $V_{OC}$  (b)  $J_{SC}$  (c) FF and (d) PCE with thickness of absorber layer and  $N_A$ .

maintains a relatively steady value of approximately 82.44 % across various  $N_D$  and thickness, except for  $N_D$  ranging from  $1 \times 10^{19}$  to  $1 \times 10^{20} \text{ cm}^{-3}$ . Within a thickness range of 100 to 800 nm, first FF decreases approximately 13.46 % for the range of  $N_D$  of  $1 \times 10^{14}$  to  $1 \times 10^{16} \text{ cm}^{-3}$ . The FF shows a slight increase by around 3.27 % for the range of  $N_D$  of  $1 \times 10^{17}$  to  $1 \times 10^{19} \text{ cm}^{-3}$  and further decrease for higher value of  $N_D$ . Fig. 6(d) depicts a correlation between  $N_D$  and PCE with KGeCl<sub>3</sub> thickness. As  $N_D$  increases from  $1 \times 10^{14}$  to  $1 \times 10^{19} \text{ cm}^{-3}$ , PCE increases whereas for  $N_D$  greater than the  $1 \times 10^{19} \text{ cm}^{-3}$  which results in decrease in PCE. Hence, the optimized value of  $N_D$  is  $1 \times 10^{18} \text{ cm}^{-3}$  for KGeCl<sub>3</sub>-based PSC. Specifically, it rises from approximately 16.07 to 28.18 % with initial increment in  $N_D$  and thickness of the KGeCl<sub>3</sub> layer. The PCE decreased to 0.01 % with a high value of  $N_D$ . The high value of doping results in formation of coulomb traps, which decreases the mobility of charge carriers. So, we need to take the optimal value of  $N_D$  for simulation [43]. This pattern suggests a direct relationship between  $N_D$  and PCE, with a more pronounced effect at higher concentrations. It is evident that increasing  $N_D$  of KGeCl<sub>3</sub> absorber layer has no discernible impact on the  $V_{OC}$  value, particularly when the concentrations are below  $1 \times 10^{20} \text{ cm}^{-3}$ , across each individual thickness. This could be attributed to the complete formation of the depletion width, impacting the

generation rate of charge carriers and the diffusion length of minority carrier's holes in ETL and electrons in HTL. Conversely, the  $V_{OC}$  value increases with the thickness of KGeCl<sub>3</sub> for each value of  $N_A$ . This phenomenon can be ascribed to the prolonged lifetime and enhanced length of charge collection, resulting in greater photogenerated current. Consequently, leakage current and recombination rate decreases as the KGeCl<sub>3</sub> thickness grows [44]. The PCE values encapsulate the overall performance of  $V_{OC}$ ,  $J_{SC}$  and FF, with its value primarily influenced by  $V_{OC}$  and FF shown below in Fig. 6.

### 3.1.3. Effect of acceptor carrier concentration ( $N_A$ ) with thickness

Fig. 7 illustrates a contour plot showcasing the change in the photovoltaic parameters with respect to two key factors: thickness of KGeCl<sub>3</sub> ranging from 100 to 800 nm and  $N_A$  ranging from  $1 \times 10^{14}$  to  $1 \times 10^{21} \text{ cm}^{-3}$ . From Fig. 7(a), it is evident that the  $V_{OC}$  shows improvement, increasing from 0.96 to 1.34 V as  $N_A$  enhances from  $1 \times 10^{14}$  to  $1 \times 10^{21} \text{ cm}^{-3}$ . Meanwhile, there is only a minor change in the  $V_{OC}$  values with increase in KGeCl<sub>3</sub> thickness. In Fig. 7(b), it is analyzed that the value of  $J_{SC}$  increases from approximately 17.71 to 30.60 mA/cm<sup>2</sup> as  $N_A$  rises from  $1 \times 10^{14}$  to  $1 \times 10^{21} \text{ cm}^{-3}$  for increase in thickness of KGeCl<sub>3</sub>. However, the value of  $J_{SC}$  remains constant around 17.71 mA/cm<sup>2</sup> for

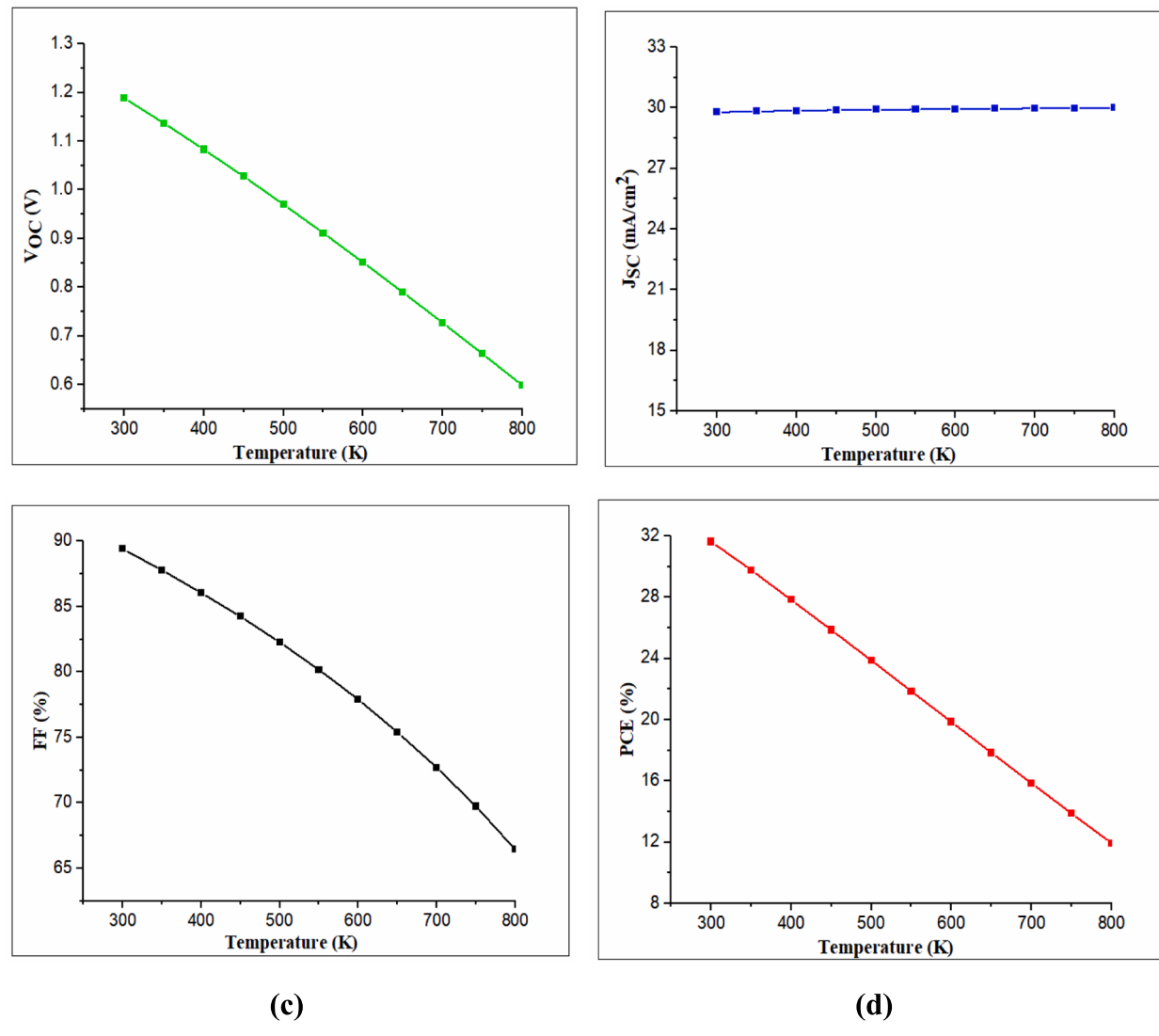


**Fig. 8.** The QE curves of the simulated PSC as a function of absorber layer (a) thickness, (b)  $E_g$ , (c)  $N_D$  and (d)  $N_A$ .

$N_A$  ranging from  $1 \times 10^{14}$  to  $1 \times 10^{21} \text{ cm}^{-3}$  at constant thickness of KGeCl<sub>3</sub>. From Fig. 7(c), it can be inferred that the FF values generally remain constant at around 88 % across various  $N_A$  and thicknesses. However, there is an exception: for  $N_A$  ranging from  $1 \times 10^{14}$  to  $1 \times 10^{21} \text{ cm}^{-3}$  and thickness of the absorber layer between 100 to 500 nm, the FF increases from approximately 76.48 to 90.58 %. Additionally, a higher FF value of about 91 % is achieved for  $N_A$  of  $1 \times 10^{21} \text{ cm}^{-3}$  and for various thickness ranging from 100 to 800 nm. In Fig. 7(d), it is evident that the PCE increases from 16.56 % to 28.63 % as  $N_A$  rises from  $1 \times 10^{14}$  to  $1 \times 10^{17} \text{ cm}^{-3}$ , accompanied by an increase in thickness. Subsequently, as  $N_A$  further increases from  $1 \times 10^{17}$  to  $1 \times 10^{21} \text{ cm}^{-3}$ , the value of PCE rises from 17.50 % to 31.10 %. These findings may be rationalized by the increase in carrier concentration leading to heightened electron diffusion from the KGeCl<sub>3</sub> layer to ETL. This elevated electron diffusion subsequently augments the device's built-in voltage ( $V_{bi}$ ), predominantly formed by the depletion width, consequently resulting in a significant rise in  $V_{OC}$  [42,45]. However, the  $J_{SC}$  values improve with increasing  $N_A$  due to enhancement of photogenerated

charge carriers and the reduction of both leakage current and recombination current, particularly noticeable for KGeCl<sub>3</sub> thickness exceeding 300 nm. These simulation results conclude that the optimized value of  $N_A$  is  $1 \times 10^{19} \text{ cm}^{-3}$  for KGeCl<sub>3</sub>-based PSC.

In this instance, the shape of PCE closely mirrors  $J_{SC}$ , as the  $N_A$  predominantly affects the photogenerated current. Consequently, the QE is measured as a function of thickness of absorber layer,  $E_g$  and carrier concentration, as illustrated in Fig. 8. It's apparent that QE exhibits a different shape for the different values of thickness, reaching 50 % at 300 nm and 100 % at 800 nm. As the  $E_g$  increases from 1.30 to 1.55 eV, the region under the curve representing higher QE shifts downward from 1000 to 800 nm depicted in Fig. 8(b). The Fig. 8(c) showed that the  $N_D$  is raised from  $1 \times 10^{14}$  to  $1 \times 10^{20} \text{ cm}^{-3}$ , the QE value enhances from approximately 50 to 98 % across wavelengths from 300 to 640 nm. Conversely, the QE value declines from 98 to 34 % for longer wavelengths from 640 to 880 nm. The QE value falls from 99 to 4 % for all further wavelengths at  $N_D$  of  $1 \times 10^{21} \text{ cm}^{-3}$ . Regardless of the  $N_A$  value, the QE maintains consistent values and shapes demonstrated in Fig. 8

Fig. 9. Impact of temperature on PV parameters of KGeCl<sub>3</sub> PSC.

**Table 4**  
Effect of change in temperature on PV parameters.

Temperature	V <sub>OC</sub> (V)	J <sub>SC</sub> (mA/cm <sup>2</sup> )	FF (%)	PCE (%)
300 K	1.188	29.78	89.39	31.64
350 K	1.136	29.83	87.78	29.78
400 K	1.083	29.86	86.05	27.84
450 K	1.027	29.89	84.23	25.87
500 K	0.970	29.91	82.27	23.88
550 K	0.911	29.93	80.17	21.87
600 K	0.851	29.95	77.91	19.86
650 K	0.789	29.96	75.39	17.84
700 K	0.727	29.98	72.70	15.85
750 K	0.663	29.99	69.74	13.88
800 K	0.598	30.00	66.44	11.93

(d). The findings suggest that the photogenerated current increases with high-energy photons but decreases for lower-energy ones, indicating differing rates of charge generation and recombination that influence J<sub>SC</sub>. These results confirm and support the notion that PCE is primarily affected by J<sub>SC</sub> [46]. Based on the simulations, it can be inferred that the KGeCl<sub>3</sub> E<sub>g</sub>, thickness, N<sub>D</sub> and N<sub>A</sub> should fall within the ranges of 1.40 eV, 600 nm,  $1 \times 10^{18} \text{ cm}^{-3}$  and  $1 \times 10^{19} \text{ cm}^{-3}$ , respectively to attain higher PCE.

### 3.2. Effect of temperature on PSC

To examine the impact of operating temperature on the PV parameters, WS<sub>2</sub> is used as ETL and PEDOT: PSS as HTL as illustrated in Fig. 9. The operating temperature at which the PSC operates has been varied between 300 K and 800 K depicted in Table 4. Fall in the performance with temperature increase is related to a decrease in diffusion length of charge carriers [47]. Several solar cell architectures show the instability of their overall performance due to deformation among layers at high temperatures. In KGeCl<sub>3</sub>-based PSC, fall in efficiency with temperature is about 63 %, for thickness of ETL and HTL is 100 nm and 80 nm respectively. When the enhancement of temperature occurs, the PCE drops significantly from 31.64 % at 300 K to 11.93 % at 800 K. The sharp fall in PCE shows that the optimized device is highly unstable towards higher values of temperature. The minor rise in J<sub>SC</sub> with increasing temperature results in reduced E<sub>g</sub> and creation of additional e<sup>-</sup>h<sup>+</sup> pairs [48]. The value of V<sub>OC</sub> is decreasing with an increase in the operating temperature with increasing interfacial defects and series resistance. The decrease in diffusion length with increase in temperature, leading to a rise in series resistance, which in turn impacts the FF and overall PCE of the device [49,50]. The increment in temperature results in enhancement in reverse saturation current and recombination rate of charge carriers, therefore the V<sub>OC</sub>, FF and PCE decreased [51,52]. The simulation outcomes showed that the optimized value of temperature is

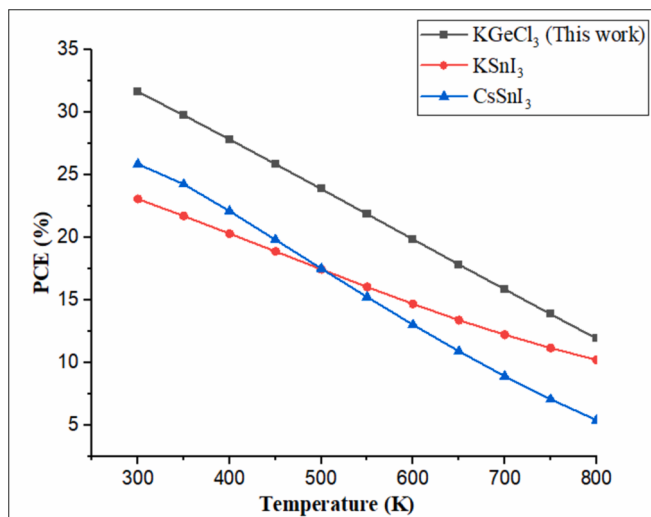


Fig. 10. PCE vs temperature curves of various PSC materials [53,54].

300 K. Comparison of observed temperature dependence with PCE of different PSC materials is shown below in Fig. 10.

### 3.3. Verification with respect to the ideal cell

The comparison of the obtained PV parameters of KGeCl<sub>3</sub>-based PSC as a function of absorber layer E<sub>g</sub> with the ideal single junction solar cell parameters has been done. The maximum PCE of 29.82 % with V<sub>OC</sub> of 1.19 V, J<sub>SC</sub> of 30.08 mA/cm<sup>2</sup>, and FF of 82.74 % for the optimized configuration of FTO/WS<sub>2</sub>/KGeCl<sub>3</sub>/PEDOT: PSS/Au has been obtained at E<sub>g</sub> of 1.49 eV and radiative recombination coefficient of 10<sup>-12</sup> cm<sup>3</sup>/sec. The ideal single junction solar cell parameters are as follows: PCE of 31.00 %, V<sub>OC</sub> of 1.20 V, J<sub>SC</sub> of 29.80 mA/cm<sup>2</sup>, and FF of 89.80 % at the absorber layer E<sub>g</sub> of 1.50 eV [55]. This demonstrated that the work outcomes are within the limit of the ideal single junction solar cell parameters.

## 4. Conclusions

This work comprises simulation study of KGeCl<sub>3</sub>-based PSC. The effect of distinct parameters, including thickness of absorber layer, ETLs and HTLs, E<sub>g</sub>, N<sub>D</sub>, N<sub>A</sub> and operating temperature have been examined using SCAPS-1D. The study demonstrated PEDOT: PSS as a promising HTL that could replace the expensive and less-conductive Spiro-OMeTAD. The maximum PCE of 29.82 % was obtained for the configuration of FTO/WS<sub>2</sub>/KGeCl<sub>3</sub>/PEDOT: PSS/Au. The SCAPS-1D outcomes, deduced that the optimized thickness of the absorber layer was 600 nm, with N<sub>D</sub> of  $1 \times 10^{18}$  cm<sup>-3</sup> and a N<sub>A</sub> of  $1 \times 10^{19}$  cm<sup>-3</sup> results in maximum PCE at E<sub>g</sub> of 1.40 eV. The optimized PSC is simulated at N<sub>t</sub> of  $1 \times 10^{15}$  cm<sup>-3</sup>. The simulation trend demonstrated that photovoltaic performance of a PSC falls with increment in operating temperature hence 300 K is optimized temperature. The device PCE improved beyond 29 % by optimizing thickness, operating temperature, E<sub>g</sub>, N<sub>D</sub> and N<sub>A</sub>. The proper optimization of suitable ETL and HTL has been done for KGeCl<sub>3</sub>-based PSC hence, this can be an alternative to Pb-based PSC for the preparation of efficient, low-cost and eco-friendly PSCs.

## CRediT authorship contribution statement

**Rahul Kundara:** Writing – original draft, Visualization, Methodology, Investigation, Formal analysis, Data curation, Conceptualization. **Sarita Baghel:** Writing – review & editing, Validation, Supervision, Resources, Formal analysis.

## Declaration of competing interest

The authors declare that they have no known competing financial interests or personal relationships that could have appeared to influence the work reported in this paper.

## Acknowledgment

The author, Rahul Kundara is thankful to Delhi Technological University, New Delhi for providing a senior research fellowship. We are very grateful to Marc Burgelman, the Electronics and Information Systems (ELIS), University of Gent, Belgium, for providing us with SCAPS-1D software.

## References

- [1] M.S. Islam, K. Sobayel, A. Al-Kahtani, M.A. Islam, G. Muhammad, N. Amin, M. Shahiduzzaman, M. Akhtaruzzaman, Defect study and modelling of SnX3-based perovskite solar cells with SCAPS-1D, Nanomater. 11 (2021), <https://doi.org/10.3390/nano11051218>.
- [2] A. Singha, A. Paul, S. Koul, V. Sharma, S. Mallick, K.R. Balasubramaniam, D. Kabra, Stable and Efficient Large Area 4T Si/perovskite Tandem Photovoltaics with Sputtered Transparent Contact, Sol. RRL. 7 (2023) 2300117, <https://doi.org/10.1002/solr.202300117>.
- [3] J. Jeong, M. Kim, J. Seo, H. Lu, P. Ahlawat, A. Mishra, Y. Yang, M.A. Hope, F. T. Eickemeyer, M. Kim, Y.J. Yoon, Pseudo-halide anion engineering for  $\alpha$ -FAPbI<sub>3</sub> perovskite solar cells, Nature. 592 (2021) 381–385, <https://doi.org/10.1038/s41586-021-03406-5>.
- [4] Y. Tang, Z. Gu, C. Fu, Q. Xiao, S. Zhang, Y. Zhang, Y. Song, FAPbI<sub>3</sub> Perovskite Solar cells: From Film morphology regulation to device optimization, Sol. RRL. 6 (2022) 2200120, <https://doi.org/10.1002/solr.202200120>.
- [5] C. Liang, Z. Huang, J. Su, L. Shi, S. Liang, Y. Dong, Study on Performance Optimization of Perovskite Solar Cells Based on MAPbI<sub>3</sub>, Adv. Theor. Simul. 7 (2024) 2301015, <https://doi.org/10.1002/adts.202301015>.
- [6] Y. Liu, Y. Liu, Y. Guo, Organic-inorganic hybrid perovskite materials and their application in transistors, Mater. Chem. Front. 7 (2023) 5215–5246, <https://doi.org/10.1039/D3QM00697B>.
- [7] A. Kojima, K. Teshima, Y. Shirai, T. Miyasaka, Organometal halide perovskites as visible-light sensitizers for photovoltaic cells, J. Am. Chem. Soc. 131 (2009) 6050–6051, <https://doi.org/10.1021/ja809598r>.
- [8] N.G. Park, Perovskite solar cells: an emerging photovoltaic technology, Mater. Today. 18 (2015) 65–72, <https://doi.org/10.1016/j.mattod.2014.07.007>.
- [9] Y. Zhao, K. Zhu, Organic-inorganic hybrid lead halide perovskites for optoelectronic and electronic applications, Chem. Soc. Rev. 45 (2016) 655–689, <https://doi.org/10.1039/C4CS00458B>.
- [10] M. Kulbak, D. Cahen, G. Hodes, How important is the organic part of lead halide perovskite photovoltaic cells? Efficient CsPbBr<sub>3</sub> cells, J. Phys. Chem. Lett. 6 (2015) 2452–2456, <https://doi.org/10.1021/acs.jpclett.5b00968>.
- [11] G.E. Eperon, S.D. Stranks, C. Menelaou, M.B. Johnston, L.M. Herz, H.J. Snaith, Formamidinium lead trihalide: a broadly tunable perovskite for efficient planar heterojunction solar cells, Energy Environ. Sci. 7 (2014) 982–988, <https://doi.org/10.1039/C3EE4382H>.
- [12] N.A. Oquendo, Y. Chen, Y.Y. Xiao, Q. Meng, C.B. Han, H. Yan, Y. Zhang, Stability of all-inorganic perovskite solar cells, Nano Energy. 67 (2020) 104249, <https://doi.org/10.1016/j.nanoen.2019.104249>.
- [13] N. Sun, S. Fu, Y. Li, L. Chen, J. Chung, M.M. Saeed, K. Dolia, A. Rahimi, C. Li, Z. Song, Y. Yan, Tailoring Crystallization Dynamics of CsPbI<sub>3</sub> for Scalable Production of Efficient Inorganic Perovskite Solar Cells, Adv. Funct. Mater. 34 (2024) 2309894, <https://doi.org/10.1002/adfm.202309894>.
- [14] J. Zhuang, J. Wang, F. Yan F, Review on chemical stability of lead halide perovskite solar cells, Nano-Micro Letters. 15 (2023) 84. doi: 10.1007/s40820-023-01046-0.
- [15] S. Gressler, F. Part, S. Scherhauser, G. Obersteiner, M. Huber-Humer, Advanced materials for emerging photovoltaic systems—Environmental hotspots in the production and end-of-life phase of organic, dye-sensitized, perovskite, and quantum dots solar cells, Sustain. Mater. Technol. 34 (2022) e00501. doi: 10.1016/j.susmat.2022.e00501.
- [16] G. Schileo, G. Grancini, Lead or no lead? Availability, toxicity, sustainability and environmental impact of lead-free perovskite solar cells, J. Mater. Chem. c. 9 (2021) 67–76, <https://doi.org/10.1039/DOTC04552G>.
- [17] N.K. Noel, S.D. Stranks, A. Abate, C. Wehrenfennig, S. Guarnera, A.A. Haghhighirad, A. Sadhanala, G.E. Eperon, S.K. Pathak, M.B. Johnston, A. Petrozza, L.M. Herz, H. J. Snaith, Lead-free organic-inorganic tin halide perovskites for photovoltaic applications, Energy Environ. Sci. 7 (2014) 3061–3068, <https://doi.org/10.1039/c4ee01076k>.
- [18] M.G. Ju, M. Chen, Y. Zhou, H.F. Garces, J. Dai, L. Ma, N.P. Padture, X.C. Zeng, Earth-Abundant Nontoxic Titanium(IV)-based Vacancy-Ordered Double Perovskite Halides with Tunable 1.0 to 1.8 eV Bandgaps for Photovoltaic Applications, ACS Energy Lett. 3 (2018) 297–304, <https://doi.org/10.1021/acsenergylett.7b01167>.

- [19] Z. Zhang, X. Li, X. Xia, Z. Wang, Z. Huang, B. Lei, Y. Gao, High-Quality (CH<sub>3</sub>NH<sub>3</sub>)<sub>3</sub>Bi<sub>2</sub>I<sub>9</sub> Film-Based Solar Cells: Pushing Efficiency up to 1.64%, *J. Phys. Chem. Lett.* 8 (2017) 4300–4307, <https://doi.org/10.1021/acs.jpclett.7b01952>.
- [20] M. Wang, P. Zeng, S. Bai, J. Gu, F. Li, Z. Yang, M. Liu, High-Quality Sequential-Vapor-Deposited Cs<sub>2</sub>AgBiBr<sub>6</sub> Thin Films for Lead-Free Perovskite Solar Cells, *Sol. RRL.* 2 (2018) 1800217, <https://doi.org/10.1002/solr.201800217>.
- [21] Y. Zong, Y. Zhou, Y. Zhang, Z. Li, L. Zhang, M.G. Ju, M. Chen, S. Pang, X.C. Zeng, N. P. Padture, Continuous Grain-Boundary Functionalization for High-Efficiency Perovskite Solar Cells with Exceptional Stability, *Chem.* 4 (2018) 1404–1415, <https://doi.org/10.1016/j.chempr.2018.03.005>.
- [22] M.A. Siddique, A.S. Rahman, The SCAPS-1D simulation of non-toxic KGeCl<sub>3</sub> perovskite from DFT derived properties, *Mater. Sci. Eng. b.* 303 (2024) 117268, <https://doi.org/10.1016/j.mseb.2024.117268>.
- [23] N. Shrivastav, M.A. Hamid, J. Madan, R. Pandey, Exploring KGeCl<sub>3</sub> material for perovskite solar cell absorber layer through different machine learning models, *Sol. Energy.* 278 (2024) 112784, <https://doi.org/10.1016/j.solener.2024.112784>.
- [24] K. Sekar, L. Marasamy, S. Mayarambakkam, H. Hawashin, M. Nour, J. Bouclé, Lead-free, formamidinium germanium-antimony halide (FA 4 GeSbCl 12) double perovskite solar cells: the effects of band offsets, *RSC Adv.* 13 (2023) 25483–25496, <https://doi.org/10.1039/D3RA03102K>.
- [25] V. Kumar, R. Kumar, F. Chand, Performance analysis of ecofriendly Ge based perovskite solar cell using computational approach, *Materials Letters.* 361 (2024) 136145, <https://doi.org/10.1016/j.matlet.2024.136145>.
- [26] M.S. Azizman, A.W. Azhari, D.S. Halin, N. Ibrahim, S. Sepeai, N.A. Ludin, M. Nor, I.N. Ho, Progress in tin-germanium perovskite solar cells: A review, *Synthetic Metals.* 299 (2023) 117475, <https://doi.org/10.1016/j.synmet.2023.117475>.
- [27] A. Kuddus, M.F. Rahman, S. Ahmed, J. Hossain, A.B.M. Ismail, Role of facile synthesized V<sub>2</sub>O<sub>5</sub> as hole transport layer for CdS/CdTe heterojunction solar cell: Validation of simulation using experimental data, *Superlattices Microstruct.* 132 (2019) 106168, <https://doi.org/10.1016/j.spmi.2019.106168>.
- [28] U. Mandadapu, S.V. Vedanayakam, K. Thyagarajan, Simulation and analysis of lead based perovskite solar cell using SCAPS-1D, *Indian Journal of Science and Technology.* 10 (2017) 65–72, <https://doi.org/10.17485/jst/2017/v11i10/110721>.
- [29] F. Azri, A. Meftah, N. Sengouga, A. Meftah, Electron and hole transport layers optimization by numerical simulation of a perovskite solar cell, *Sol. Energy.* 181 (2019) 372–378, <https://doi.org/10.1016/j.solener.2019.02.017>.
- [30] K.D. Jayan, V. Sebastian, Comprehensive device modelling and performance analysis of MASnI<sub>3</sub> based perovskite solar cells with diverse ETM, HTM and back metal contacts, *Sol. Energy.* 217 (2021) 40–48, <https://doi.org/10.1016/j.solener.2021.01.058>.
- [31] M.K. Hossain, G.F.I. Toki, A. Kuddus, M.H.K. Rubel, M.M. Hossain, H. Bencherif, M.F. Rahman, M.R. Islam, M. Mushtaq, An extensive study on multiple ETL and HTL layers to design and simulation of high-performance lead-free CsSnCl<sub>3</sub>-based perovskite solar cells, *Sci Rep.* 13 (2023) 2521, <https://doi.org/10.1038/s41598-023-28506-2>.
- [32] H. Wei, P. Qiu, Y. Li, Y. He, M. Peng, X. Zheng, X. Liu, Challenges and strategies of all-inorganic lead-free halide perovskite solar cells, *Ceram. Int.* 48 (2022) 5876–5891, <https://doi.org/10.1016/j.ceramint.2021.11.184>.
- [33] S. Rai, B.K. Pandey, D.K. Dwivedi, Modeling of highly efficient and low cost CH<sub>3</sub>NH<sub>3</sub>Pb(I-xCl<sub>x</sub>)<sub>3</sub> based perovskite solar cell by numerical simulation, *Opt. Mater.* 100 (2020) 109631, <https://doi.org/10.1016/j.optmat.2019.109631>.
- [34] S.Z. Haider, H. Anwar, M. Wang, Theoretical device engineering for high-performance perovskite solar cells using CuSCN as hole transport material boost the efficiency above 25%, *Phys. Status Solidi (a).* 216 (2019) 1900102 <https://doi.org/10.1002/pssa.201900102>.
- [35] A.A. Kanoun, M.B. Kanoun, A.E. Merad, S. Goumri-Said, Toward development of high-performance perovskite solar cells based on CH<sub>3</sub>NH<sub>3</sub>Gel<sub>3</sub> using computational approach, *Sol. Energy.* 182 (2019) 237–244, <https://doi.org/10.1016/j.solener.2019.02.041>.
- [36] S. Bhattacharai, T.D. Das, Optimization of carrier transport materials for the performance enhancement of the MgAl<sub>3</sub> based perovskite solar cell, *Sol. Energy.* 217 (2021) 200–207, <https://doi.org/10.1016/j.solener.2021.02.002>.
- [37] I.M. De Los Santos, H.J. Cortina-Marrero, M.A. Ruiz-Sánchez, L. Hechavarria-Difur, F.J. Sánchez-Rodríguez, M. Courel, H. Hu, Optimization of CH<sub>3</sub>NH<sub>3</sub>PbI<sub>3</sub> perovskite solar cells: A theoretical and experimental study, *Sol. Energy.* 199 (2020) 198–205. doi: 10.1016/j.solener.2020.02.026.
- [38] S. Kohnehpoushi, P. Nazari, B.A. Nejand, M. Eskandari, MoS<sub>2</sub>: a two-dimensional hole-transporting material for high-efficiency, low-cost perovskite solar cells, *Nanotechnol.* 29 (2018) 205201, <https://doi.org/10.1088/1361-6528/aa1d4>.
- [39] D. Ompong, J. Singh, High open-circuit voltage in perovskite solar cells: The role of hole transport layer, *Org. Electron.* 63 (2018) 104–108, <https://doi.org/10.1016/j.orgel.2018.09.006>.
- [40] T. Ouslimane, L. Et-Taya, L. Elmaimouni, A. Benami, Impact of absorber layer thickness, defect density, and operating temperature on the performance of MAPbI<sub>3</sub> solar cells based on ZnO electron transporting material, *Heliony.* 7(3) (2021) e06379. doi: 10.1016/j.heliyon.2021.e06379.
- [41] M. Asaduzzaman, M. Hasan, A.N. Bahar, An investigation into the effects of band gap and doping concentration on Cu (In, Ga) Se 2 solar cell efficiency, *SpringerPlus.* 5 (2016) 1–8, <https://doi.org/10.1186/s40064-016-2256-8>.
- [42] M. Abdelfatah, J. Ledig, A. El-Shaer, A. Wagner, V. Marin-Borras, A. Sharafeev, P. Lemmens, M.M. Mosaad, A. Waag, A. Bakin, Fabrication and characterization of low cost Cu<sub>2</sub>O/ZnO: Al solar cells for sustainable photovoltaics with earth abundant materials, *Sol. Energy Mater. Sol. Cells.* 145 (2016) 454–461, <https://doi.org/10.1016/j.solmat.2015.11.015>.
- [43] Z. Shang, T. Heumueller, R. Prasanna, G.F. Burkhardt, B.D. Naab, Z. Bao, M. D. McGehee, A. Salles, Trade-off between trap filling, trap creation, and charge recombination results in performance increase at ultralow doping levels in bulk heterojunction solar cells, *Adv. Energy Mater.* 6 (2016) 1601149, <https://doi.org/10.1002/aenm.201601149>.
- [44] K.P. Musselman, A. Marin, L. Schmidt-Mende, J.L. MacManus-Driscoll, Incompatible length scales in nanostructured Cu<sub>2</sub>O solar cells, *Adv. Funct. Mater.* 22 (2012) 2202–2208, <https://doi.org/10.1002/adfm.201102263>.
- [45] W.M. Lin, N. Yazdani, O. Yarema, S. Volk, M. Yarema, T. Kirchartz, V. Wood, Simulating nanocrystal-based solar cells: A lead sulfide case study, *J. Chem. Phys.* 151 (2019) 241104, <https://doi.org/10.1063/1.5129159>.
- [46] M. Abdelfatah, A.M. El Sayed, W. Ismail, S. Ulrich, V. Sittinger, A. El-Shaer, SCAPS simulation of novel inorganic ZrS<sub>2</sub>/Cu<sub>2</sub>O heterojunction solar cells, *Sci. Rep.* 13 (2023) 4553, <https://doi.org/10.1038/s41598-023-31553-4>.
- [47] G. Pindolia, S.M. Shinde, P.K. Jha, Optimization of an inorganic lead free RbGeI<sub>3</sub> based perovskite solar cell by SCAPS-1D simulation, *Sol. Energy.* 236 (2022) 802–821, <https://doi.org/10.1016/j.solener.2022.03.053>.
- [48] V. Deswal, S. Kaushik, R. Kundara, S. Baghel, Numerical simulation of highly efficient Cs<sub>2</sub>AgInBr<sub>6</sub>-based double perovskite solar cell using SCAPS 1-D, *Mater. Sci. Eng. b.* 299 (2024) 117041, <https://doi.org/10.1016/j.mseb.2023.117041>.
- [49] M.K. Hossain, M.H. Rubel, G.I. Toki, I. Alam, M.F. Rahman, H. Bencherif, Effect of various electron and hole transport layers on the performance of CsPbI<sub>3</sub>-based perovskite solar cells: A numerical investigation in DFT, SCAPS-1D, and wxAMPS frameworks, *ACS Omega.* 7 (2022) 43210–43230, <https://doi.org/10.1021/acsomega.2c05912>.
- [50] R. Kundara, S. Baghel, Device modelling of lead free (CH<sub>3</sub>NH<sub>3</sub>)<sub>2</sub>CuX<sub>4</sub> based perovskite solar cells using SCAPS simulation, *Opt. Quantum Electron.* 55 (2023) 968, <https://doi.org/10.1007/s11082-023-05244-3>.
- [51] S. Ahmed, F. Jannat, M.A.K. Khan, M.A. Alim, Numerical development of eco-friendly Cs<sub>2</sub>TiBr<sub>6</sub> based perovskite solar cell with all-inorganic charge transport materials via SCAPS-1D, *Optik.* 225 (2021) 165765, <https://doi.org/10.1016/j.ijleo.2020.165765>.
- [52] A. Chen, K. Zhu, Computer simulation of a-Si/c-Si heterojunction solar cell with high conversion efficiency, *Sol. Energy.* 86 (2012) 393–397, <https://doi.org/10.1016/j.solener.2011.10.015>.
- [53] G. Pindolia, S.M. Shinde, P.K. Jha, Non-leaded, KS<sub>n</sub>I<sub>3</sub> based perovskite solar cell: A DFT study along with SCAPS simulation, *Mater. Chem. Phys.* 297 (2023) 127426, <https://doi.org/10.1016/j.matchemphys.2023.127426>.
- [54] M. Jiang, J. Tang, Simulated development and optimized performance of narrow-bandgap CsSnI<sub>3</sub>-based all-inorganic perovskite solar cells, *J. Phys. d: Appl. Phys.* 54 (2021) 465104, <https://doi.org/10.1088/1361-6463/ac1e4c>.
- [55] A. Morales-Acevedo, Fundamentals of solar cell physics revisited: Common pitfalls when reporting calculated and measured photocurrent density, open-circuit voltage, and efficiency of solar cells, *Sol. Energy.* 262 (2023) 111774, <https://doi.org/10.1016/j.solener.2023.05.051>.